DOI: 10.53660/CLM-1617-23I17

CFD Simulation of isothermal upward two-phase flow in a vertical annulus using interfacial area transport equation

Simulação Computacional de fluxo bifásico ascendente isotérmico em um anel vertical usando a equação de transporte de área interfacial

Received: 2023-06-08 | Accepted: 2023-07-12 | Published: 2023-07-17

Flavio Eduardo Ceravolo
ORCID: https://orcid.org/0000-0002-8990-5425
Instituto de Pesquisas Energéticas e Nucleares-IPEN/USP, Brazil
E-mail: flavioceravolo@gmail.com
Marcelo da Silva Rocha
ORCID: https://orcid.org/0000-0003-2445-1298
Instituto de Pesquisas Energéticas e Nucleares-IPEN/USP, Brazil
E-mail: msrocha@ipen.br
Roberto Navarro de Mesquita
ORCID: https://orcid.org/0000-0002-5355-0925
Instituto de Pesquisas Energéticas e Nucleares-IPEN/USP, Brazil
E-mail: rnavarro@ipen.br
Delvonei Alves de Andrade
ORCID: https://orcid.org/0000-0002-6689-3011
Instituto de Pesquisas Energéticas e Nucleares-IPEN/USP, Brazil
E-mail: delvonei@ipen.br

ABSTRACT

This work presents a numerical simulation of a vertical, upward, isothermal two-phase flow of air bubbles and water in an annular channel applying a Computational Fluid Dynamics (CFD) code. For this, the Two-Fluid model is applied considering interfacial force correlations, namely: drag, lift, wall lubrication, turbulent dispersion, and virtual mass. The turbulence k-ε model effects and the influence of One-group Interfacial Area Transport Equation (IATE) are taken into account, in this case, the influence of two source term correlations for the bubble breakup and coalescence IATE is analysed. The work assesses whether the code properly represents the physical phenomenon by comparing the simulation results with experimental data obtained from the literature. Six flow conditions are evaluated based on two superficial liquid velocities and three void fractions in the bubbly flow regimen. The annular channel adopted has an outer pipe with an internal diameter of 38.1 mm and an inner cylinder of 19.1 mm. To represent this geometry, a three-dimensional mesh was generated with 160,000 elements, after a mesh sensitivity study. The void fraction distribution, taken radially to the flow section, is the main parameter analysed as well as interfacial area concentration, interfacial gas velocity, and bubble sizes distribution. The CFD model implemented in this work demonstrates satisfactory agreement with the reference experimental data but indicates the need for further improvement in the phase interaction models.

Keywords: Bubble column; Two-phase flow; Annular channel; CFD; Interfacial area concentration

RESUMO

Este trabalho apresenta uma simulação numérica de um escoamento bifásico vertical, ascendente e isotérmico de bolhas de ar e água em um canal anular aplicando um código de Dinâmica dos Fluidos Computacional (CFD). O modelo de Dois Fluidos é aplicado considerando as correlações de forças interfaciais, a saber: arrasto, sustentação, lubrificação da parede, dispersão turbulenta e massa virtual. Os efeitos do modelo k-ε de turbulência e a influência da Equação de Transporte de Área Interfacial de Um Grupo (IATE) são levados em consideração, neste caso, a influência de duas correlações de termos de fonte para o rompimento e coalescência de bolhas IATE é analisada. O trabalho avalia se o código representa adequadamente o fenômeno físico comparando os resultados da simulação com dados experimentais obtidos na literatura. Seis condições de fluxo são avaliadas com base em duas velocidades superficiais de líquido e três frações de vazio no regime de fluxo borbulhante. O canal anular adotado possui um tubo externo com diâmetro interno de 38,1 mm e um cilindro interno de 19,1 mm. Para representar esta geometria, uma malha tridimensional foi gerada com 160.0000 elementos, após um estudo de sensibilidade da malha. A distribuição da fração de vazio, tomada radialmente à seção de escoamento, é o principal parâmetro analisado, assim como a concentração da área interfacial, a velocidade do gás na interface e a distribuição do tamanho das bolhas. O modelo CFD implementado neste trabalho demonstra concordância satisfatória com os dados experimentais de referência, indicando a necessidade de melhorias nos modelos de interação de fase.

Palavras-chave: Coluna de bolhas; Escoamento bifásico, Canal anular, CFD, Concentração de área interfacial

INTRODUCTION

Two-phase flow in annular channel can be found in several industrial applications such as the flow of oil and gas in exploration well, chemical reactors, double-tube heat exchangers, or even can represent the subchannel of a water-cooled nuclear reactor core (Hibiki et al. (2003)). The study of two-phase isothermal flow in the bubble regime in annular channels can be applied to complex systems involving the interaction between the flowing phases and with the channel walls. For instance, in nuclear reactors, the study of phase change in the fuel coolant requires the application of concepts developed with air-water flows in simplified geometries like circular, annular, and rectangular channels. These studies are employed for the development of numerical models capable of representing physical phenomena involving phase migration, coalescence phenomena, bubble fragmentation, and turbulence effects.

Currently, due to the increased processing power of personal computers, commercial tools of CFD (Computational Fluid Dynamics) have gained evidence in the industry and the research area as a tool to understand many two-phase flow phenomena. The ability of CFD to deal with complex three-dimensional geometries, simulating local effects that could not be treated by traditional tools, such as experimental techniques, is one of the main reasons for the intensive use of CFD in many studies.

Today, CFD models can solve problems in single-phase flows with a high level of accuracy, however, concerning multiphase phenomena, this tool is still under development, requiring the improvement of numerical models and validation of these models with experimental data under more comprehensive conditions (van Wachem & Almstedt (2003)).

At the industrial scale, the usual approach for multiphase flow modelling with CFD applies the commonly referred two-fluid model (Ishii & Hibiki (2011)), which is analogous to the RANS model for single phase. This model is based on a separate treatment of each flow phase in a continuous medium. For this, two sets of conservation equations of mass, energy, and momentum are written. However, due to the interaction between the phases, closure relations at the interface are needed, as a way to properly couple the two sets of equations. Closure relationships are semi-empirical models that account for forces acting on phases such as drag force, lift force, wall lubrication force, virtual mass force, and turbulent dispersion force. The dynamics of these forces dictate the distribution of the phases in a given flow. Additionally, the magnitude of interactions between the phases is closely related to the amount of interfacial area available in the medium, as well as to local transfer mechanisms such as the intensity of the turbulence processes in the proximity of interfaces and the bubble breakup and coalescence mechanisms. Therefore, properly estimating the interfacial area concentration (IAC) is of fundamental importance in the two-fluid model.

Another promising approach, the Direct Numerical Simulation (DNS), has been used in multiphase systems, however, demanding computational resources that are not too accessible to the majority of practical applications. Due to this fact, the use of the Eulerian-Eulerian or two-fluid model is the most widely employed technique in commercial CFD software as it provides a reasonable balance between accuracy and computational effort in two-phase modelling (Sharma et al. (2019)).

This work aims to apply a CFD commercial code, Ansys Fluent 19.0, to the representation of an isothermal rising air-water flow in an annulus channel. For this, experimental data presented in the work of Hibiki et al. (2003) are used as comparison parameters.

MATHEMATICAL MODELLING OF TWO-PHASE FLOWS

The mathematical model is based on the two-fluid model approach, which is divided into a set of equations for each phase describing the conservation of mass, conservation of momentum, energy, turbulence phenomena, and interaction between the phases.

Mass Conservation Equation

The continuity of mass for each phase k, disregarding the mass transfer at the interface, is given by:

$$\frac{\partial}{\partial t}(\alpha_k \rho_k) + \nabla \cdot (\alpha_k \rho_k \mathbf{v}_k) = 0 \quad (1)$$

since it is assumed valid for the isothermal air-water flow. The term α_k represents the volume fraction of phase k, ρ_k its density, and $\mathbf{v}_k$ corresponds to the phase velocity.

Momentum Conservation Equation

The momentum balance of each phase is given by:

$$\frac{\partial}{\partial t}(\alpha_k \rho_k \mathbf{v}_k) + \nabla \cdot (\alpha_k \rho_k \mathbf{v}_k \mathbf{v}_k) = -\alpha_k \nabla P - \nabla \cdot (\alpha_k \boldsymbol{\tau}_\mathbf{k}) + \alpha_k \rho_k \mathbf{g} + \mathbf{F} \quad (2)$$

where the term P is the pressure at which the phases are subjected, g the gravity acceleration, **F** stands for the external forces acting over the phases, and $\boldsymbol{\tau}_\mathbf{k}$ is the stress tensor given by:

$$\boldsymbol{\tau}_\mathbf{k} = -\mu_{eff,L}[(\nabla \mathbf{v}_k) + (\nabla \mathbf{v}_k{}^T) - \frac{2}{3}(\nabla \mathbf{v}_k)\,\mathbf{I}] \quad (3)$$

Here the term I is the unit tensor, and $\mu_{eff,L}$ is the effective viscosity of the liquid according to:

$$\mu_{eff,L} = \mu_L + \mu_{T,L} + \mu_{BIT,L} \quad (4)$$

The terms μ_L, $\mu_{T,L}$ and $\mu_{BIT,L}$ correspond respectively to the molecular viscosity, the viscosity resulting from turbulence, and viscosity due to the bubble-induced turbulence (BIT).

For the gas phase the effective viscosity, $\mu_{eff,G}$, is given by the following ratio:

$$\mu_{eff,G} = \mu_{eff,L} \frac{\rho_G}{\rho_L} \tag{5}$$

where ρ_G and ρ_L are the gas and liquid phase densities.

Modelling the Interfacial Forces

In the two-fluid model, the interfacial transfer phenomena, such as mass, momentum, and energy transfer, strongly depend on the adopted closure relationships. To take into account these phenomena, five interfacial momentum sources terms **F**, have been considered in Eq. (2): drag force, lift force, wall lubrication force, virtual mass force, and turbulent dispersion force. The following sections address the models applied to describe each source term.

Drag Force

A particle flowing in a liquid medium is subjected to drag and lift forces. The drag force arises parallel and in the opposite direction to the flow, while the lift force, arises orthogonally to the flow. The drag momentum source depends on the relative velocity between the phases, as it is given by:

$$\mathbf{F}_D = \frac{3}{4}\frac{C_D}{d_b}\alpha_G \rho_L |\mathbf{v}_G - \mathbf{v}_L|(\mathbf{v}_L - \mathbf{v}_G) \tag{6}$$

Here, the chosen correlation to describe the drag coefficient C_D is based on the work of Schiller & Naumann (1935) which is an acceptable method for all fluid-fluid pairs, according to Ansys (2013). In this model, the drag force coefficient depends on the bubble Reynolds number as stated by:

$$C_D = \begin{cases} \frac{24}{Re_b}(1 + 0.15 Re_b^{0.687}) & Re_b \leq 1000 \\ 0.44 & Re_b > 1000 \end{cases} \tag{7}$$

where the bubble Reynolds number, Re_b, is defined by:

$$Re_b = \frac{\rho_L |\mathbf{v}_G - \mathbf{v}_L| d_b}{\mu_L} \tag{8}$$

Lift Force

In a vertical upward flow, a bubble experiences a force pointing perpendicularly to the flow direction, mainly due to the velocity gradients in the liquid phase. Here the momentum source, related to lift force, is modelled according to the work of Drew & Lahey (1993), as follows:

$$\mathbf{F}_{lift,L} = -\mathbf{F}_{lift,G} = -C_l \rho_L \alpha_G (\mathbf{v}_L - \mathbf{v}_G) \times (\nabla \times \mathbf{v}_L) \tag{9}$$

where C_l is the lift force coefficient, ρ_L is the density of the liquid phase, α_G the volumetric fraction of the gas phase, $\mathbf{v_L}$ the velocity of the liquid phase and $\mathbf{v_G}$ the velocity of the gas phase.

In order to calculate the lift coefficient C_l, here is considered the correlation of Tomiyama et al. (2002) which applies to ellipsoidal, spherical, and cap bubbles. For spherical bubbles the model generates a positive coefficient, forcing the bubbles to the wall, while for large and distorted bubbles, a negative coefficient is generated forcing the bubbles to the core of the channel, according to the following equation:

$$C_l = \begin{cases} \text{mín.}\left[0.288\tanh\left(0.121\text{Re}_p\right), f(\text{Eo}')\right] & \text{Eo}' \leq 4 \\ f(\text{Eo}') & 4 < \text{Eo}' \leq 10 \\ -0.27 & \text{Eo}' > 10 \end{cases} \quad (10)$$

wherein the above equation f(Eo') is given by:

$$f(\text{Eo}') = 0.00105\text{Eo}'^3 - 0.0159\text{Eo}'^2 - 0.0204\text{Eo}' + 0.474 \quad (11)$$

This correlation is based on the modified Eötvös number Eo' given by:

$$\text{Eo}' = \frac{g(\rho_L - \rho_G)d'^2_b}{\sigma} \quad (12)$$

where d'_b is the largest dimension of a deformed bubble, as follows:

$$d'_b = d_b(1 + 0.163\text{Eo}^{0.757})^{1/3} \quad (13)$$

The usual Eötvös number, Eo represents the relationship between the thrust forces and the surface tension forces on a bubble subject to a liquid medium, as given by the equation below:

$$\text{Eo} = \frac{g(\rho_L - \rho_G)d_b^2}{\sigma} \quad (14)$$

where σ is the surface tension, g is the acceleration of gravity, and d_b is the bubble diameter.

For a more realistic physical representation of the void fraction near the wall, the hypothesis developed by Shaver & Podowski (2015) is taken into account in the lift force model. It consists of a correction in the lift coefficient next to the wall, based on the spherical geometry of the bubbles. The correlation proposed by the author is presented in the following equation:

$$C_{lc} = \begin{cases} 0 & \frac{y_w}{d_b} < \frac{1}{2} \\ C_l\left[3\left(\frac{2y_w}{d_b} - 1\right)^2 - 2\left(\frac{2y_w}{d_b} - 1\right)^3\right] & \frac{1}{2} \leq \frac{y_w}{d_b} \leq 1 \\ C_l & \frac{y_w}{d_b} > 1 \end{cases} \quad (15)$$

where C_{lc} represents the corrected value of the lift force coefficient due to the proximity to the wall. The value of y_w is the distance from the wall and d_b the bubble diameter. It can be observed that for wall distances less than half bubble diameter the correlation dumps the lift coefficient C_l, while for regions ranging between half bubble diameter and one bubble diameter, a parabolic adjust is used, and for distances greater than one bubble diameter the actual value of C_l is applied. In the work of Lubchenko et al. (2018), due to the high void fraction results obtained adjacent to the wall (i.e. much smaller than the bubble diameter), the correlation of Shaver & Podowski (2015) was successfully employed in addition to a specific model for turbulence dispersion force. A similar approach was considered by Feng & Bolotnov (2017) to simulate the wall forces due to the drainage around the bubbles close to the walls. Recently, the Shaver & Podowski (2015) correlation was adopted by Colombo & Fairweather (2019), Sugrue et al. (2017), and Marfaing et al. (2018), providing satisfactory accuracy for void fraction and gas velocity profiles when compared to experimental data. In order to incorporate the effects of C_{lc}, a user-defined function (UDF) was programmed and implemented in the CFD model.

Wall Lubrication Force

When a bubble moves in an infinite liquid media the flow of liquid around the bubble is approximately symmetrical, however, when a wall appears in the vicinity of the bubble, the no-slip condition on the wall decreases the flow of liquid between the bubble and the wall, which increases the flow on the opposing surface of the bubble. This creates an asymmetry in the flow around the bubble and, consequently, a hydrodynamic force that pushes the gas phase away from the wall, acting in the opposite direction to the lift force, is expressed by:

$$\mathbf{F}_{wl} = C_{wl}\rho_L\alpha_G\left|(\mathbf{v}_L - \mathbf{v}_G)_{||}\right|^2 \times \mathbf{n}_w \tag{16}$$

where C_{wl} is the wall lubrication coefficient, ρ_L the liquid phase density, α_G the gas phase volumetric fraction, $(\mathbf{v}_L\text{-}\mathbf{v}_G)_{||}$ stands for the phase relative velocity tangential to the wall, and $\mathbf{n}_w$ is the normal vector pointing away from the wall.

The correlation adopted for calculating the wall lubrication coefficient, C_{wl} is also derived from the work of Antal et al. (1991) given by:

$$C_{wl} = \max\left(0, \frac{C_{w1}}{d_b} + \frac{C_{w2}}{y_w}\right) \tag{17}$$

where the values of the coefficients C_{w1} and C_{w2} are respectively -0.01 and 0.05 and the values of d_b and y_w correspond to the diameter of the bubble and the nearest distance from the wall. The result of Eq. (17) will only be different from zero if it satisfies the condition expressed by:

$$y_w \leq -\left(\frac{C_{w2}}{C_{w1}}\right) d_b \tag{18}$$

Therefore, considering the above values of C_{w1} and C_{w2}, it means that $y_w \leq 5d_b$, indicating the need for sufficiently refined discretization meshes close to the wall.

Virtual Mass Force

When a particle accelerates in a continuous medium, as in the case of an air bubble in a liquid mass, this requires that the mass of the continuous medium surrounding the particle also accelerates in the same proportion, for this, there must be a force to allow such action. The effect is analogous to that of assigning a virtual mass to the bubble.

According to Ishii & Hibiki (2011) and Yeoh & Tu (2010), the virtual mass force becomes significant in situations where the dispersed phase density is much lower than that of the continuous phase, such as air-water flow. In addition to this, according to Ishii & Hibiki (2011) studies have shown that the use of the virtual mass force model has improved the stability of numerical models of multiphase flow.

As described above, the effect of virtual mass force occurs when the gas phase accelerates relatively to the liquid phase, therefore according to Drew & Lahey (1990), this effect is accounted by:

$$\mathbf{F}_{vm,G} = -\mathbf{F}_{vm,L} = 0.5\alpha_G\rho_L\left(\frac{d_L(\mathbf{v}_L)}{dt} - \frac{d_G(\mathbf{v}_G)}{dt}\right) \tag{19}$$

where each derivative term, with respect to the time, is generically given by:

$$\frac{d(\varphi)}{dt} = \frac{\partial(\varphi)}{\partial t} + (\mathbf{v}\cdot\nabla)\varphi \tag{20}$$

Turbulent Dispersion Force

Turbulence in a two-phase flow creates erratic or fluctuating behaviour in the relative velocity between the phases. Physically, the meaning of turbulent dispersion is a result of the fluctuating of the component of the forces acting on the bubbles. In the simplest case, the turbulent dispersion force at one point is the average of the fluctuating component of the drag force components whose trajectories are inserted at this point (Lopez de Bertodano et al. (2006)). In a liquid-gas flow in a vertical bubble column, this force acts on the dispersion of the bubbles in the direction perpendicular to the flow, "flattening" the phase profiles.

The model applied in this work to describe the turbulence dispersion force is given by Lopez de Bertodano (1991) as:

$$\mathbf{F}_{td,L} = -\mathbf{F}_{td,G} = C_{TD}\,\rho_L\,k_L\nabla\alpha_G \tag{21}$$

where ρ_L is the liquid density, k_L is turbulent kinetic energy, $\nabla\alpha_G$ is the gas volume fraction gradient and C_{TD} is an empirical constant whose default value is 1.0, however, according to Lahey & Drew (2001), this parameter has been adjusted between 0.1 and 1.0. Here, the turbulent dispersion constant, C_{TD} was adjusted to the value of 0.2.

Turbulence Models

The turbulence is modelled using an adaptation of the standard k-ε model Launder & Spalding (1972) for two-phase flow, as given by Ansys (2013). This model takes into account the transport of the liquid phase turbulence kinetic energy, k, and the turbulence energy dissipation rate, ε weighted with liquid phase volume fraction.

$$\frac{\partial}{\partial t}(\alpha_L \rho_L k_L) + \nabla \cdot (\alpha_L \rho_L \mathbf{v}_L k_L) = \nabla \cdot \left(\alpha_L \left(\mu_L + \frac{\mu_{T,L}}{\sigma_k}\right) \nabla k_L\right) + \alpha_L G_{k,L} - \alpha_L \rho_L \varepsilon_L + S_{k,L} \quad (22)$$

$$\frac{\partial}{\partial t}(\alpha_L \rho_L \varepsilon_L) + \nabla \cdot (\alpha_L \rho_L \mathbf{v}_L \varepsilon_L) = \nabla \cdot \left(\alpha_L \left(\mu_L + \frac{\mu_{T,L}}{\sigma_\varepsilon}\right) \nabla \varepsilon_L\right) + \alpha_L \frac{\varepsilon_L}{k_L}\left(C_{1\varepsilon} G_{k,L} - C_{2\varepsilon} \rho_L \varepsilon_L\right) + \alpha_L \rho_L S_{\varepsilon,L} \quad (23)$$

In the above equations, for the liquid phase, α_L is the volumetric fraction, ρ_L the density, ε_L the turbulent dissipation rate, $\mathbf{v}_L$ is the phase-weighted velocity, μ_L the molecular viscosity, and $\mu_{T,L}$ the turbulent viscosity is given by:

$$\mu_{T,L} = \rho_L C_\mu \frac{{k_L}^2}{\varepsilon_L} \quad (24)$$

The following constants are considered C_μ=0.09, $C_{1\varepsilon}$=0.09, $C_{2\varepsilon}$=0.09, σ_k=1, and σ_ε=1. The parameters $S_{k,L}$ and $S_{\varepsilon,L}$ refer to the source terms due to bubble-induced turbulence (BIT), which in the present work are replaced by the model Sato & Sekoguchi (1975), as follows:

$$\mu_{BIT,L} = C_{\mu,G} \rho_L \alpha_G d_b |\mathbf{v}_G - \mathbf{v}_L| \quad (25)$$

This model simply incorporates the BIT effect, by an additional viscosity term based on relative phases velocities. This way, both effects of $\mu_{T,L}$, and $\mu_{BIT,L}$ comprise the effective viscosity of the liquid phase, $\mu_{eff,L}$, as previously presented in Eq. (4). The recommended value for $C_{\mu,G}$ is 0.6 according to Sato & Sekoguchi (1975). As recently pointed out in the work of Sharma et al. (2019), the k-ε turbulence model combined with the model of Sato & Sekoguchi (1975) for BIT, has been widely applied in two-phase flow works, some of which being Lopez de Bertodano et al. (1994), Krepper et al. (2007), Prabhudharwadkar et al. (2012) and Sharma et al. (2017).

Interfacial Area Concentration Model

In the multiphase phenomena, the transfer of mass, momentum, and energy are closely related to the interfacial area available in the media and to a driving force (Kocamustafaogullari & Ishii (1995)). Therefore, in mathematical modelling, this quantity is taken as a property named Interfacial Area Concentration (IAC) which is the ratio between the available area of interface and the volume. The following equation represents the IAC transport model:

$$\frac{\partial}{\partial t}(\rho_G X) + \nabla(\rho_G \mathbf{v}_G X) = \frac{1}{3}\frac{D\rho_G}{Dt} X + \frac{2}{3}\frac{\dot{m}_G}{\alpha_G} X + \rho_G (S_{RC} + S_{WE} + S_{TI}) \quad (26)$$

where X represents the IAC, ρ_G is the gas density, and α_G the gas volume fraction. The first two terms on the right hand of Eq. (26) stand for the expansion due to the compressibility and mass transfer respectively. The parameters S_{RC}, S_{WE}, and S_{TI} correspond to the source terms due to the bubble interaction: random collision, wake entrainment, and turbulent-induced breakage, respectively.

From the determination of IAC, it is possible to obtain the bubble mean diameter in a given region of the flow through the Sauter mean diameter, as follows:

$$d_b = \frac{6\alpha_G}{X} \tag{27}$$

The Sauter mean diameter is defined as the diameter of a sphere having the same area-to-volume ratio as the particle. In Eq. (27), the mean bubble diameter, d_b is calculated based on the ratio of void fraction α_G to the interfacial area concentration X.

IAC source terms models

In this work, the influence of two One-group IAC source terms models was evaluated. The first model from Hibiki & Ishii (2000), here called Case A, takes into account the random collision coalescence and turbulent impact breakage; the second model from Wu et al. (1998) and Ishii & Kim (2001), here stated as Case B, additionally considers the wake entrainment coalescence effect.

The following Eqs. (28) and (29), describe the source terms from the correlation of Hibiki & Ishii (2000), which considers the mechanism of bubble coalescence due to random collisions and the bubble breakup due to turbulent impact, denoted by the subscripts RC and TI respectively in the following equations:

$$S_{RC} = \frac{\Gamma_C}{\psi^{11/3}} \frac{{\varepsilon_L}^{1/3}\alpha_G^2 X^{5/3}}{(\alpha_{Gmax} - \alpha_G)} \exp\left[-K_C \frac{\psi^{5/6}\rho_L^{1/2}{\varepsilon_L}^{1/3}}{\sigma^{1/2}}\left(\frac{\alpha_G}{X}\right)^{5/6}\right] \tag{28}$$

$$S_{TI} = \frac{\Gamma_B(1-\alpha_G){\varepsilon_L}^{1/3}X^{5/3}}{\psi^{11/3}\alpha_G^{2/3}(\alpha_{Gmax} - \alpha_G)} \exp\left[-\frac{K_B}{\psi^{5/3}} \frac{\sigma}{\rho_L {\varepsilon_L}^{2/3}}\left(\frac{X}{\alpha_G}\right)^{5/3}\right] \tag{29}$$

where α_G is the gas volume fraction, X the interfacial area concentration, d_b the bubble average diameter, ε_L the turbulence dissipation rate of the liquid phase (evaluated from Eq. (23)), σ the interfacial surface tension, ρ_L is the liquid density, ψ is the bubble shape factor, α_{Gmax} is the gas volume fraction to which the bubble collisions frequency will increase to infinity. The adjustable coefficients in the coalescence model are $\Gamma_C = 0.188$ and $K_C = 0.129$, for the breakup model, the adjustable coefficients are $\Gamma_B = 0.264$ and $K_B = 1.37$, and the shape factor $\psi = 6$ is taken to spherical bubbles in both models. To take into consideration the wake entrainment (WE) effect

on the bubble coalescence, besides the bubble coalescence due to random collision (RC) and break up due to turbulent impact (TI), is considered the correlation of Wu et al. (1998) and Ishii & Kim (2001) as follows:

$$S_{RC} = -\frac{1}{3\pi} C_{RC} u_t X^2 \left[\frac{1}{\alpha_{Gmax}^{1/3}(\alpha_{Gmax}^{1/3} - \alpha_G^{1/3})}\right]\left[1 - \exp\left(-C\frac{\alpha_{Gmax}^{1/3}\alpha_G^{1/3}}{\alpha_{Gmax}^{1/3} - \alpha_G^{1/3}}\right)\right] \quad (30)$$

$$S_{WE} = -\frac{1}{3\pi} C_{WE} u_r X C_D^{1/3} \quad (31)$$

$$S_{TI} = \frac{1}{18} C_{TI} u_t \frac{X^2}{\alpha_G}\left(1 - \frac{We_{cr}}{We}\right)^{1/2} \exp\left(-\frac{We_{cr}}{We}\right), \qquad We > We_{cr} \quad (32)$$

The term u_t denotes the mean bubble fluctuating velocity, given by:

$$u_t = \varepsilon^{1/3} d_b^{1/3} \quad (33)$$

where ε corresponds to the turbulence dissipation and d_b is the bubble diameter. The term u_r corresponds to the bubble terminal velocity, which is a ratio between the buoyancy and drag forces in two-phase bubbly flows, given by the following equations:

$$u_r = \left(\frac{d_b g \Delta\rho}{3 C_D' \rho_L}\right)^{1/2} \quad (34)$$

$$C_D' = 24\left(\frac{1 + 0.1 Re_D^{0.75}}{Re_D}\right) \quad (35)$$

$$Re_D = \left(\frac{\rho_L u_r d_b}{\mu_L}\right)(1 - \alpha_G) \quad (36)$$

The term g is the gravity acceleration, Δρ the phase densities difference, C_D the drag coefficient calculated by Eq. (35) with the Reynolds number Re_D, obtained in Eq. (36). The ρ_L and μ_L are the liquid density and molecular viscosity of the liquid phase.

The Weber number, We in Eq. (32), is given by:

$$We = \frac{\rho_L u_t^2 d_b}{\sigma} \quad (37)$$

As the We is bellow the critical Weber number, We_{cr}, the breakup source term, S_{TI}, tends to zero. The coefficients in the above equations here presented are C_{RC} = 0.004, C_{WE} = 0.002, C_{TI} = 0.085, C = 3.0, We_{cr} = 6.0 e α_{gmax} = 0.75.

RESULTS AND DISCUSSIONS

Geometry and Mesh Discretization

The geometry considered in the study is a one-eighth axis symmetrical section of the channel (Figure 1b). This hypothesis assumes that the flow is symmetric in the channel and aims to reduce computational effort and processing time. The annulus has a hydraulic diameter (D_h) equivalent to 19.1 mm, where the inner cylinder diameter is 19.1 mm and the outer tube internal diameter is 38.1 mm. The channel length is 1900 mm and the two measurement ports are placed on the positions Z/D_h = 40.3 and 99.0 from the inlet (Figure 1a).

Figure 1 – Schematic drawing of the annular channel (a) axial section, (b) cross-section (not to scale)

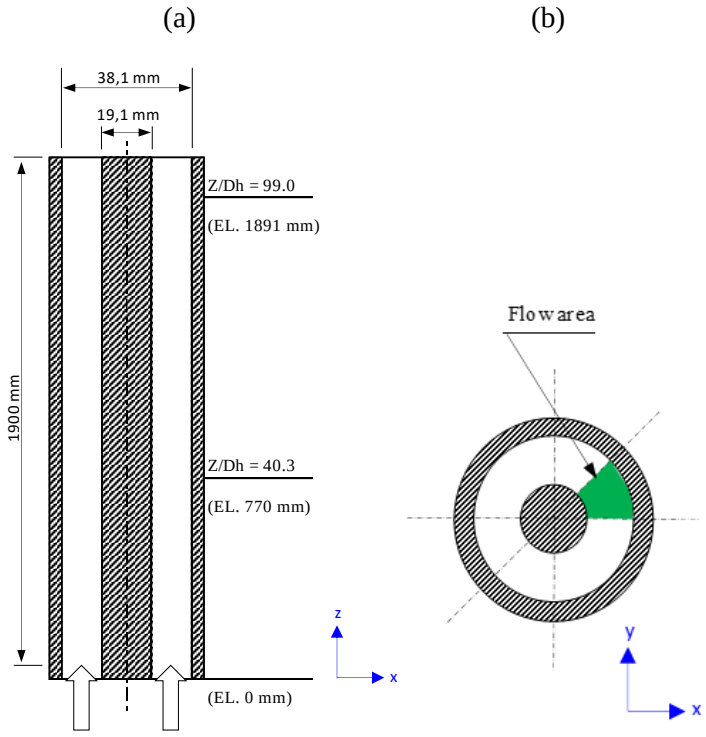

Source: Ceravolo, Rocha, Mesquita, Andrade (2020)

For the mesh construction, it was predominantly applied hexahedral control volumes with regular dimensions for the greater uniformity of the mesh, reduction in processing time, and better calculation stability. The mesh discretization proposed is shown in Figure 2.

Figure 2 – Mesh discretization in the CFD model. (a) Perspective view, and (b) Bottom view

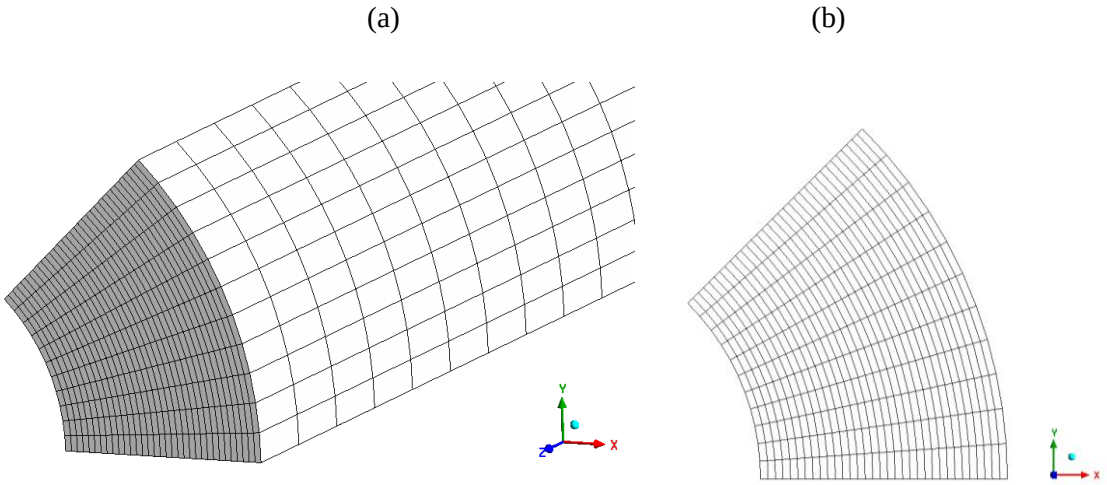

Source: Ceravolo, Rocha, Mesquita, Andrade (2020)

To establish the degree of refinement a mesh sensitivity analysis was carried out based on the methodology of Stern et al. (2001). A sufficient resolution, to represent the phase distribution in the cross-section of the annulus, was found with a 161,898 elements mesh, evenly distributed as 33 divisions in the radial, 11 divisions in the azimuthal, and 446 divisions in the axial direction.

Boundary Conditions

The simulation results were compared with experimental data from Hibiki et al. (2003), where a set of typical bubbly flow conditions were selected as boundary inlet conditions to the simulation code. The summary of these data is presented in Table 1.

Table 1 – Inlet boundary conditions based on experimental data

Parameter	**Flow conditions**					
Void fraction, α_G [-]	0.05 (●)	0.10 (▲)	0.15 (■)	0.05 (●)	0.10 (▲)	0.15 (■)
Superf. liquid velocity, j_L [m s^{-1}]	0.5160	0.5160	0.5160	1.0300	1.0300	1.0300
Superf. gas velocity, j_G [m s^{-1}]	0.0406	0.0687	0.1030	0.0683	0.1300	0.2010
IAC, X [m^{-1}]	100	175	245	110	200	290

Source: Ceravolo, Rocha, Mesquita, Andrade (2020), adapted from Hibiki et al. (2003)

The input data consist of three void fractions, α_G, at two superficial liquid velocities, j_L, and equivalent superficial gas velocities, j_G. The IAC data at the inlet is the same as declared by the author of the experimental data, Hibiki et al. (2003). For the outlet boundary condition,

constant atmospheric pressure is set. At the inlet, the boundary condition assumes flat profiles for all the flowing parameters. The fluid is an isothermal air-water mixture at 20°C and atmospheric pressure, without mass transfer between gas and liquid phase. On the inner and outer walls of the annular channel the free-slip condition is taken for the gas phase, while for the liquid phase, the no-slip condition is applied as proposed by Yeoh & Tu (2010), Lee et al. (2013), and Rzehak & Krepper (2013).

According to Hibiki et al. (2003), the data presented in Table 1 are predominantly taken at bubbly flow regimens. In order to obtain more detailed information regarding the flow pattern used as input data for the simulation, the flow map of Kelessidis & Dukler (1989), which applies to two-phase flow in a vertical annulus, was overlapped with the superficial liquid and gas velocities and presented in Figure 3.

Figure 3 – Superficial velocities at inlet boundary conditions plotted over the flow map for concentric annulus

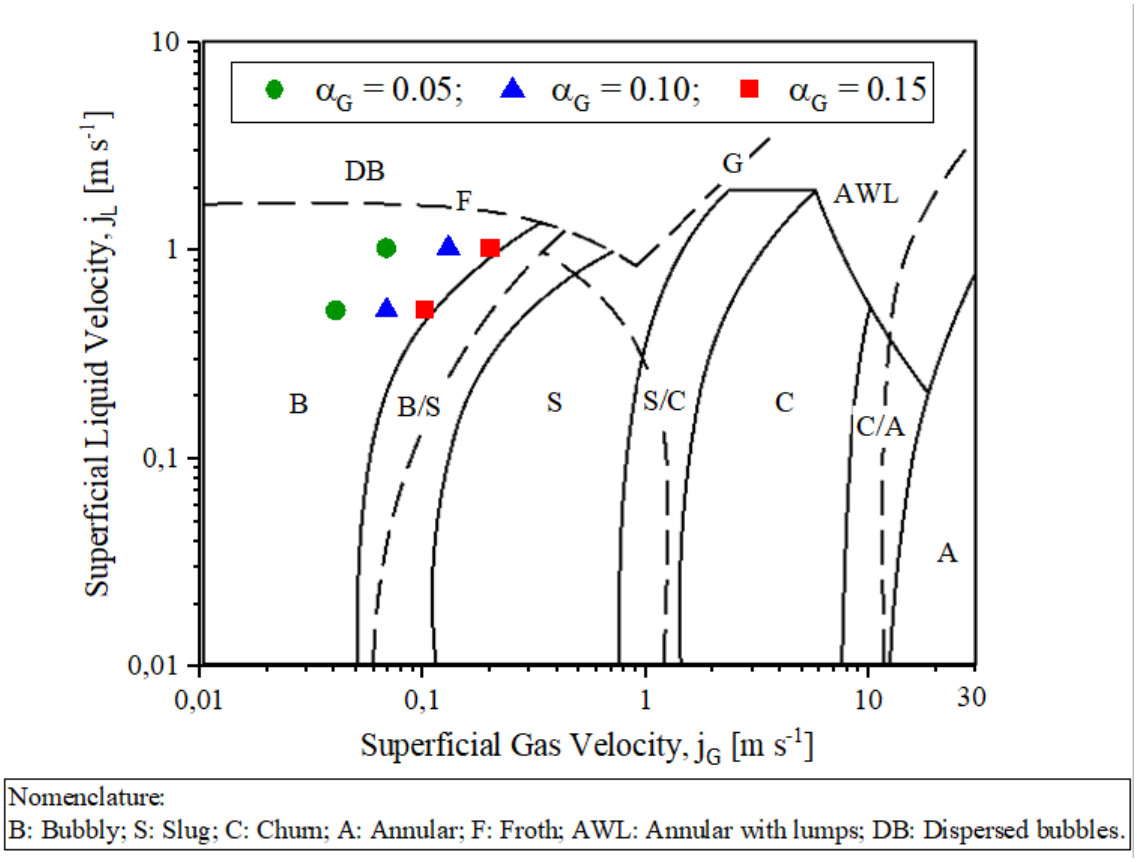

Source: Ceravolo, Rocha, Mesquita, Andrade (2020), adapted from Kelessidis & Dukler (1989)

Figure 3 shows that the low void fraction data (α_G = 0.05 and 0.10) are predominantly in the bubbly flow region (B), while the high void fraction (α_G = 0.15) data are close to the transition from bubbly to slug flow (B/S).

Simulation Results

Figure 4 through Figure 7 present the simulation results taken at elevations z/D_h = 40.3 and 99.0 from the inlet, these are the same elevations where the measurement ports were positioned by Hibiki et al. (2003) in his experiments. The radial profiles obtained from the simulation are for void fraction, IAC, bubble size diameter, and interfacial velocity. For comparison reasons, the experimental data are shown together with the simulation results.

In order to evaluate the influence of the one-group IAC source term models on the results in the CFD simulation, two cases have been considered. Case A employs the correlation of Hibiki & Ishii (2000) which considers the mechanisms of bubble breakup, due to the turbulent eddies, and the coalescence, due to random collisions. Case B applies the correlation of Wu et al. (1998) and Ishii & Kim (2001) which includes the wake entrainment process, due to the relative motion of the bubbles, as an additional coalescence mechanism. According to Hibiki & Ishii (2000), the wake entrainment process is usually more relevant when the bubbly flow condition is close to the transition from bubbly to slug, and in small diameter tubes at low flow velocities. Therefore, as the high volume fraction boundary conditions are close to the bubbly-to-slug transition (see Figure 3), it is considered relevant to evaluate the influence of the wake entrainment in the IAC transport equation.

Void Fraction Profiles

Figure 4 presents the results of void fraction profiles for the superficial liquid velocities j_L= 0.516 m s^{-1} and 1.03 m s^{-1}, and at elevations z/D_h = 40.3 and 99.0. It can be observed that the simulation results exhibit a qualitative trend similar to the experimental results since all the calculated profiles have a wall peak or intermediate wall peak shape Serizawa & Kataoka (1988) as observed in the experimental data. However, some discrepancies, mainly close to the channel wall, are observed.

Figure 4 – Simulation results and experimental data of Hibiki et al. (2003) of Void Fraction for six boundary conditions, at two elevations z/D_h = 40.3 and 99.0 from the inlet

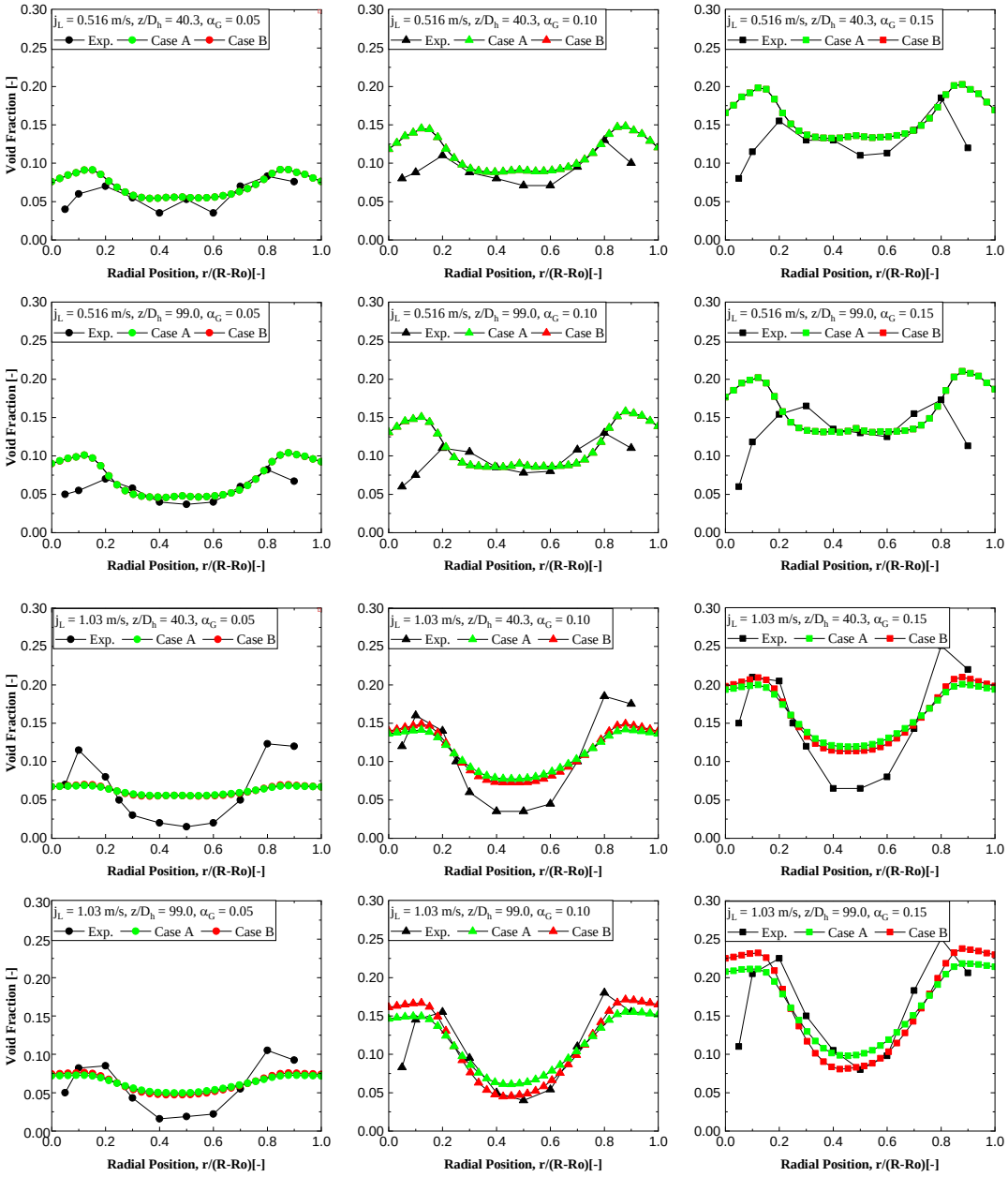

Source: Ceravolo, Rocha, Mesquita, Andrade (2020)

For the low superficial liquid velocity, j_L = 0.516 m s^{-1}, the profile in the core of the channel exhibits a good agreement with experimental data with all void fractions, however close to the walls the profiles seem to be slightly overpredicted. It is especially true for the conditions with higher void fractions. This can be related to the direct proportionality between the void fraction and the lift force expressed in Eq. (9) since this parameter will cause stronger migration of the gas phase to the walls as the gas volume fraction increases.

Comparing the results at two elevations, z/D_h = 40.3 and 99.0, at low j_L, no significant differences were revealed between the profiles, however, it can be seen an evolution in the profiles due to the actuation of the lift and wall lubrication force along the channel.

Regarding the effect of the IAC source models, denoted by Cases A and B, no appreciable effect is observed at low j_L, showing that the interactions that lead to coalescence and breakup are not playing a significant role in this condition, since the turbulence dissipative terms, ε_L, at low j_L are pretty lower than at high j_L.

Regarding the higher superficial liquid velocity, j_L = 1.03 m s^{-1}, the effect of the lift force model on the void fraction profiles is stronger than previously observed. At void fraction, α_G = 0.05 the profile is almost flat, which highly deviates from experimental data. For α_G = 0.10 and 0.15, the results better reproduced the experimental data due to the stronger lift forces produced by the model. Between the two elevations, the results at z/D_h = 99.0 show better proximity with the experimental data than at z/D_h = 40.3, especially in the core of the channel. This result may be related to the boundary conditions at the inlet that assume flat profiles for the flowing properties, and to the distance needed for the development of the flowing profile along the channel. Maybe the adoption of more realistic flowing profiles at the channel inlet could improve the profiles, however, it would require experimental data collected close to the channel inlet, which is not available in the experimental data of Hibiki et al. (2003). Regarding the influence of IAC source models, Case B tended to increase the void fraction on the wall and to reduce the void fractions in the channel core. Again, the more pronounced effect was observed for the higher void fractions and elevation z/D_h = 99.0. Both effects resulted in a greater approximation of the results with the experimental data.

IAC Profiles

In Figure 5 the IAC profiles exhibit a similar shape as the void fraction profiles since the IAC parameter is proportional to the void fraction and the bubble Sauter mean diameter which, in Figure 6, is almost constant. The relation among IAC, void fraction, and bubble diameter is expressed in Eq. (27).

At low superficial liquid velocity j_L = 0.516 m s^{-1}, the IAC profiles obtained by simulation show better proximity to experimental data than at higher superficial liquid velocity j_L = 1.03 m s^{-1}, maybe this result is related to the flat boundary conditions assumed in the inlet, as previously observed for the results of void fraction profiles.

At low void fractions, the influence of the IAC source term model is almost negligible, however, for more pronounced void fractions this influence is much stronger. The main effect of the wake entrainment model in Case B was a reduction of the IAC average magnitude, which means a higher coalescence production. It is consistent with the physical phenomena since in the higher void fraction condition, more gas phase is available in the medium, and more particles are available to interact and coalesce.

Figure 5 – Simulation results and experimental data of Hibiki et al. (2003) for IAC with six boundary conditions, at two elevations z/D_h = 40.3 and 99.0 from the inlet

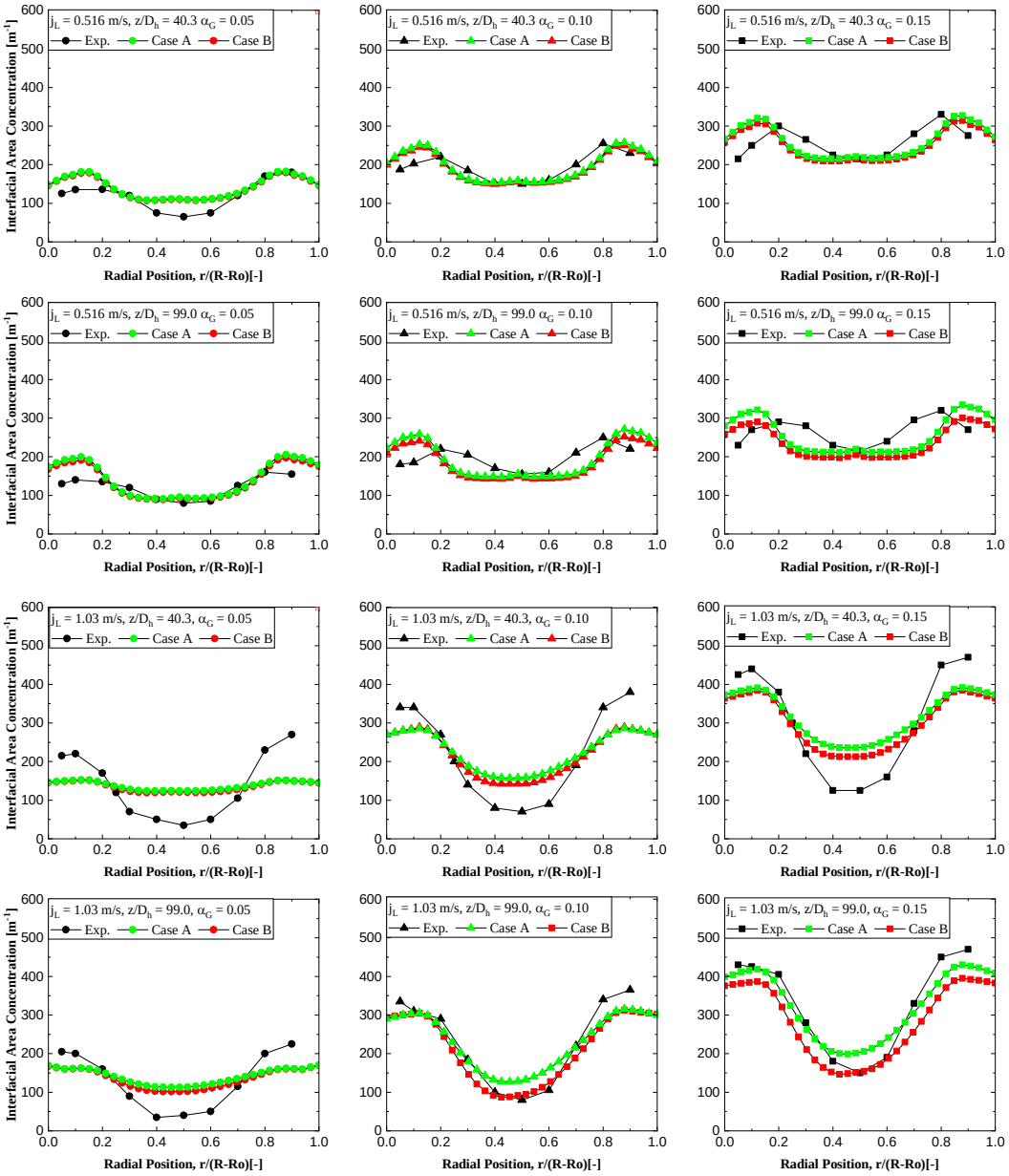

Source: Ceravolo, Rocha, Mesquita, Andrade (2020)

Bubble Sizes Profiles

In Figure 6, the simulation results present a quite constant bubble size profiles, while experimental data present smaller bubble diameters close to the walls. At first, this could be interpreted as a divergence between the simulation results and the experimental data. However, according to the author of the experimental data Hibiki et al. (2003), this reduction of bubble

diameter close to the walls is produced because only a fraction of bubble diameter can pass close to the wall (due to the bubble curvature), which results in an apparent local reduction of the Sauter mean diameter. In fact, the double-sensor conductivity probe, employed by the author, can give only a partial measurement of the bubble diameter in this region.

Regarding the influence of the IAC model in the bubble profiles, it can be seen in Figure 6 an increase in the average bubble size, mainly regarded as a higher coalescence production due to the wake entrainment effect in Case B. Besides, the coalescence is enhanced at the high void fractions since the presence of more gas-phase flowing in the medium increases the potential for bubble interaction. Furthermore, the average bubble size increases with the elevation z/D_h, since it is related to the gas expansion due to the static pressure reduction and to the holdup time, which allows for more interaction time between the bubbles.

Figure 6 – Simulation results and experimental data of Hibiki et al. (2003) for Sauter Mean Diameter of bubbles for six boundary conditions, at two elevations z/D_h = 40.3 and 99.0 from the inlet

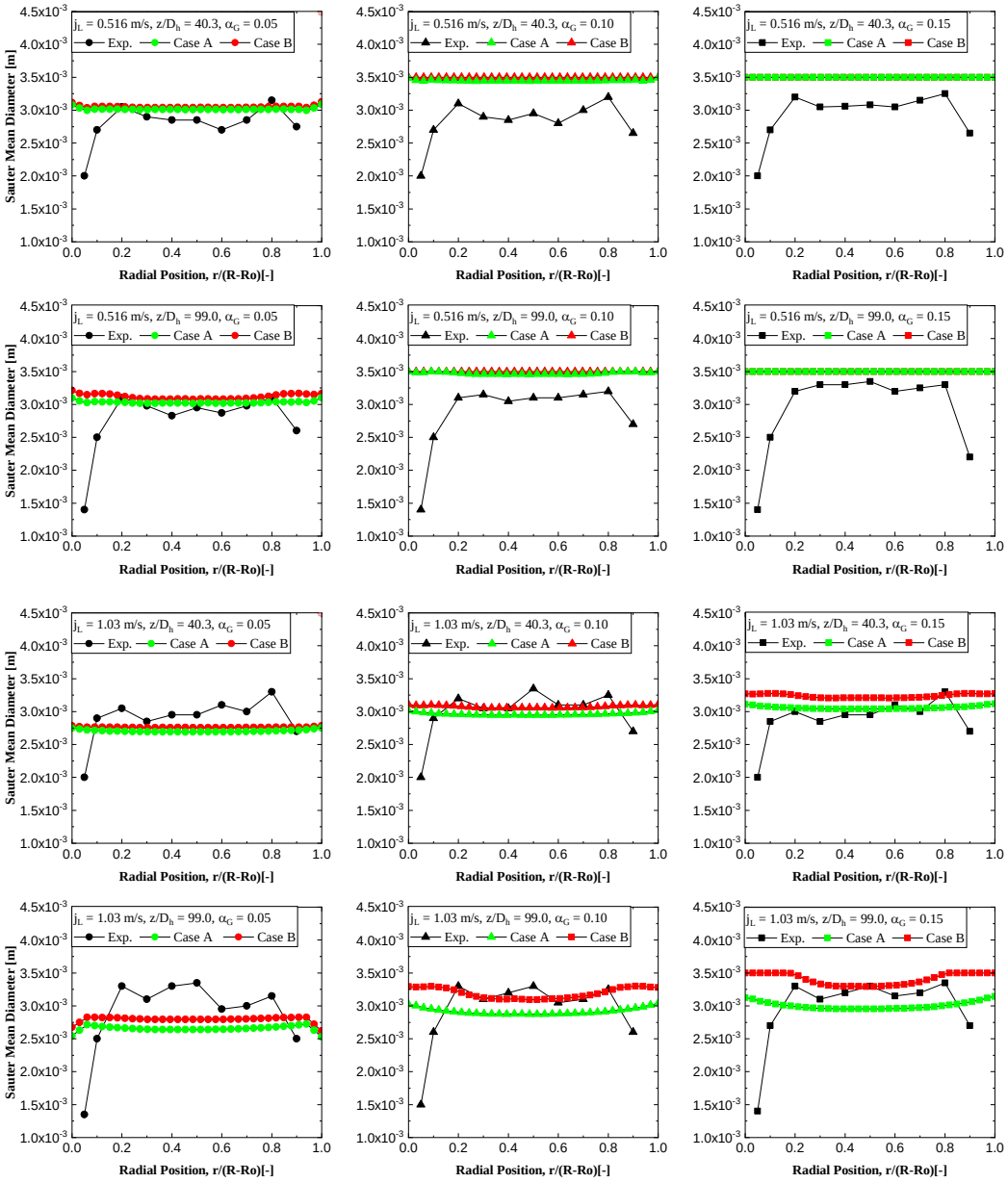

Source: Ceravolo, Rocha, Mesquita, Andrade (2020)

Velocity Profiles

In Figure 7, at low superficial liquid velocity condition j_L = 0.516 m s^{-1}, it is observed a lower interfacial velocity profile for all void fractions at both elevations.

Figure 7 – Simulation results and experimental data of Hibiki et al. (2003) for Interfacial Velocity for six boundary conditions, at two elevations z/D_h = 40.3 and 99.0 from the inlet

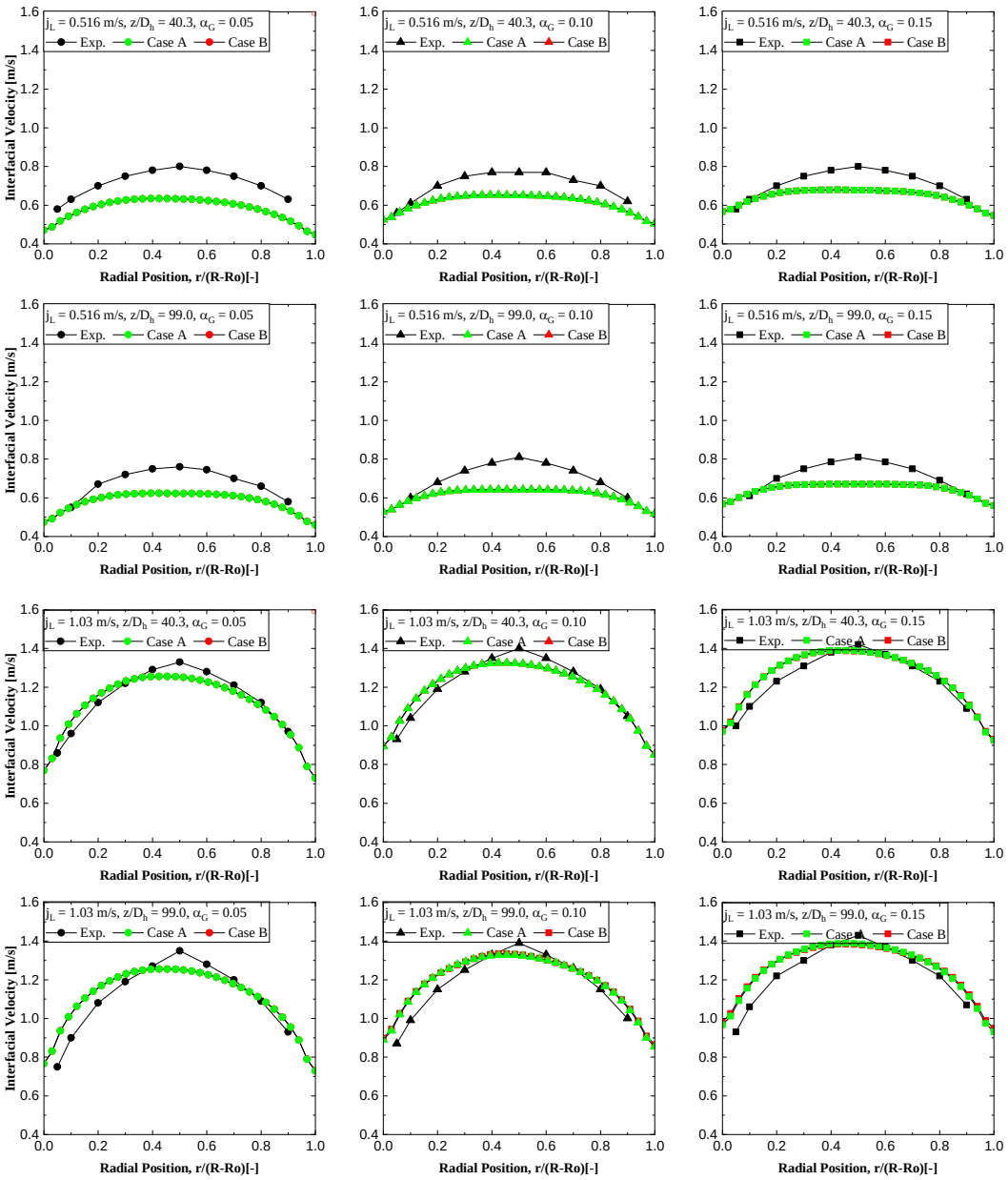

Source: Ceravolo, Rocha, Mesquita, Andrade (2020)

For the higher superficial liquid velocity condition j_L = 1.03 m s^{-1}, the results were very close to the experimental profiles. In this particular condition, in the centre of the channel, the simulation results have shown a tendency of flattening the velocity profiles, probably due to the turbulent dispersion model that intends to mimic the oscillatory movements in the secondary phase in directions perpendicular to the flow. Near the inner and outer walls, the gas phase velocity provided proximity to experimental data, showing that the assumed boundary condition of non-adherence to the wall for the gas phase provides a physically appropriate result.

In all the conditions, no significant influence of the wake entrainment source term (Case B) is observed on velocity profiles. Only in the conditions with α_G = 0.15 and 0.10, and high superficial liquid velocity, j_L = 1.03 m s^{-1} it is possible to observe a slight increase in the gas phase velocity.

CONCLUSIONS

The work carried out the simulation of an ascending isothermal two-phase flow in an annulus channel using a CFD code and evaluated the effect of two One-group IAC transport models. The numerical models employed in this work demonstrated satisfactory performance in the representation of the experimental data of the literature, revealing the potential of the CFD tool in the simulation of the two-phase in the annulus. All the flowing conditions have exhibited intermediate wall-peak behaviour, close to the inner and outer walls of the annulus, for IAC and gas volume fraction profile. The bubble diameter distributions are quite constant but close to the average bubble sizes of the experimental data. The One-group IAC model of Wu et al. (1998) and Ishii & Kim (2001), which takes into account the wake entrainment process (Case B), has increased the bubble coalescence in comparison with the IAC model of Hibiki & Ishii (2000), in Case A. Higher coalescence was observed at flow conditions approaching the bubble-slug transition where the void fraction is high. Among all flow parameters, the gas phase velocity profiles have shown the best proximity with the experimental data, however, in the core of the channel, the experimental data presents a peak gas velocity, which is not well reproduced in the simulation. Future works intend to compare further experimental data with the simulation results and investigate the influence of the turbulence models.

Notation

$C_{2\varepsilon}$	Coefficient of turbulent dissipation transport equation for the liquid phase
C_D	Drag coefficient
C'_D	Drag coefficient of wake entrainment coalescence model
C_{RC}	Empirical coefficient of random collision coalescence model
C_{TD}	Turbulent dispersion force empirical constant
C_{TI}	Empirical coefficient of turbulent impact breakup model
C_{WE}	Empirical coefficient of wake entrainment coalescence model
C_l	Lift force coefficient
C_{lc}	Corrected value of the lift force coefficient
$C_{l\varepsilon}$	Coefficient of turbulent dissipation transport equation for the liquid phase
C_{w1}	Empirical constant of wall lubrication force coefficient equation
C_{w2}	Empirical constant of wall lubrication force coefficient equation
C_{wl}	Wall lubrication force coefficient
$C_{\mu,G}$	Bubble-induced equation coefficient
d'_b	Largest dimension of a deformed bubble
d_b	Bubble diameter
D_h	Hydraulic diameter
Eo'	Modified Eötvös number
Eo	Eötvös number
$\mathbf{F}_D$	Drag force source term
$\mathbf{F}_{lift}$	Lift force source term
$\mathbf{F}_{td,G}$	Turbulent dispersion force source term
$\mathbf{F}_{vm}$	Virtual mass force source term
$\mathbf{F}_{wl}$	Wall lubrication force source term
$\mathbf{F}$	External forces acting over the phases
$G_{k,L}$	Coefficient of turbulence kinetic energy transport equation for the liquid phase
$\mathbf{g}$	Gravity acceleration
$\mathbf{I}$	Unit tensor
j_G	Gaseous phase superficial velocity
j_L	Liquid phase superficial velocity
k_L	Turbulent kinetic energy of liquid phase
K_C	Empirical coefficient of turbulent impact breakup model
$\dot{m}_G$	Mass transfer term
$\mathbf{n}_w$	Normal vector pointing away from the wall
P	Pressure

Re_b	Bubble Reynolds number
S_{RC}	IAC transport equation random collision source term
S_{TI}	IAC transport equation turbulent-induced breakage source term
S_{WE}	IAC transport equation wake entrainment source term
$S_{k,L}$	Source term of turbulence kinetic energy transport equation for the liquid phase
$S_{\varepsilon,L}$	Source term of turbulent dissipation transport equation for the liquid phase
t	Time
u_r	Bubble terminal velocity
u_t	Bubble fluctuating velocity
$\mathbf{v}_G$	Gas phase velocity
$\mathbf{v}_L$	Liquid phase velocity
$\mathbf{v}_k$	Phase k velocity
We_{cr}	Critical Weber number
X	Interfacial area concentration
y_w	Distance from the wall
z	Axial coordinate of the annular channel

Greek letters

Γ_B	Empirical coefficient of turbulent impact breakup model
Γ_C	Empirical coefficient of random collision coalescence model
α_G	Gas phase volume fraction
α_{Gmax}	Gas volume fraction of maximum bubble collisions frequency
α_L	Liquid phase volumetric fraction
α_k	Volume fraction of phase k
ε_L	Turbulent dissipation rate
$\mu_{BIT,L}$	Bubble-induced turbulence viscosity
μ_L	Molecular viscosity of the liquid
$\mu_{T,L}$	Turbulent viscosity
$\mu_{T,L}$	Turbulence viscosity
$\mu_{eff,G}$	Molecular viscosity of the gas
$\mu_{eff,L}$	Effective viscosity of the liquid
ρ_G	Gaseous phase density
ρ_L	Liquid phase density
ρ_k	Density of phase k
σ_k	Coefficient of turbulence kinetic energy transport equation
τ_k	Stress tensor

σ	Surface tension
φ	Generic variable
ψ	Bubble shape factor

REFERENCES

Ansys. (2013). *ANSYS Fluent Theory Guide* (ANSYS (ed.); Release 15). ANSYS. http://www.ansys.com

Antal, S. P., JR, R. T. L., & Flaherty, J. E. (1991). Analysis of Phase Distribution in Fully Developed Laminar Bubbly Two-Phase Flow. *International Journal of Multiphase Flow*, *17*(No.5), 635–652

Colombo, M., & Fairweather, M. (2019). Influence of multiphase turbulence modelling on interfacial momentum transfer in two-fluid Eulerian-Eulerian CFD models of bubbly flows. *Chemical Engineering Science*, *195*, 968–984. https://doi.org/10.1016/j.ces.2018.10.043

Drew, D. A., & Lahey, R. T. (1990). Some supplemental analysis concerning the virtual mass and lift force on a sphere in a rotating and straining flow. *International Journal of Multiphase Flow*, *16*(6), 1127–1130. https://doi.org/10.1016/0301-9322(90)90110-5

Drew, D. A., & Lahey, R. T. (1993). Particulate Two-Phase Flow. In *Butterworth-Heinemann Series in Chemical Engineering*. Butterworth-Heinemann (January 18, 1993)

Feng, J., & Bolotnov, I. A. (2017). Interfacial force study on a single bubble in laminar and turbulent flows. *Nuclear Engineering and Design*, *313*, 345–360. https://doi.org/10.1016/j.nucengdes.2016.12.034

Hibiki, T., & Ishii, M. (2000). One-group Interfacial Area Transport of Bubbly Flows in Vertical Round Tubes. *International Journal of Heat and Mass Transfer*, *43*(15), 2711–2726. https://doi.org/10.1016/S0017-9310(99)00325-7

Hibiki, T., Mi, Y., Situ, R., & Ishii, M. (2003). Interfacial area transport of vertical upward bubbly two-phase flow in an annulus. *International Journal of Heat and Mass Transfer*, *46*(25), 4949–4962. https://doi.org/10.1016/S0017-9310(03)00318-1

Ishii, M., & Hibiki, T. (2011). Thermo-Fluid Dynamics of Two-Phase Flow. In Intergovernmental Panel on Climate Change (Ed.), *Climate Change 2013 - The Physical Science Basis*. Springer New York. https://doi.org/10.1007/978-1-4419-7985-8

Ishii, M., & Kim, S. (2001). Micro four-sensor probe measurement of interfacial area transport for bubbly flow in round pipes. *Nuclear Engineering and Design*, *205*(1–2), 123–131. https://doi.org/10.1016/S0029-5493(00)00350-2

Kelessidis, V. C., & Dukler, A. E. (1989). Modeling flow pattern transitions for upward gas-liquid flow in vertical concentric and eccentric annuli. *International Journal of Multiphase Flow*, *15*(2), 173–191. https://doi.org/10.1016/0301-9322(89)90069-4

Kocamustafaogullari, G., & Ishii, M. (1995). Foundation of the interfacial area transport equation and its closure relations. *International Journal of Heat and Mass Transfer*, *38*(3), 481–493. https://doi.org/10.1016/0017-9310(94)00183-V

Krepper, E., Reddy Vanga, B. N., Zaruba, A., Prasser, H. M., & Lopez de Bertodano, M. A. (2007). Experimental and numerical studies of void fraction distribution in rectangular

bubble columns. *Nuclear Engineering and Design*, *237*(4), 399–408. https://doi.org/10.1016/j.nucengdes.2006.07.009

Lahey, R. T., & Drew, D. A. (2001). The analysis of two-phase flow and heat transfer using a multidimensional, four field, two-fluid model. *Nuclear Engineering and Design*, *204*(1–3), 29–44. https://doi.org/10.1016/S0029-5493(00)00337-X

Launder, B. E., & Spalding, D. B. (1972). *Lectures in Mathematical Modeling of Turbulence* (London (ed.))

Lee, D. Y., Liu, Y., Hibiki, T., Ishii, M., & Buchanan, J. R. (2013). A study of adiabatic two-phase flows using the two-group interfacial area transport equations with a modified two-fluid model. *International Journal of Multiphase Flow*, *57*, 115–130. https://doi.org/10.1016/j.ijmultiphaseflow.2013.07.008

Lopez de Bertodano, M. (1991). *Turbulent Bubbly Flow in a Triangular Duct*. Rensselaer Polytechnic Institute, Troy, New York

Lopez de Bertodano, M., Lahey, R. T., & Jones, O. C. (1994). Development of a k-ε Model for Bubbly Two-Phase Flow. *Journal of Fluids Engineering*, *116*(1), 128. https://doi.org/10.1115/1.2910220

Lopez de Bertodano, M., Sun, X., Ishii, M., & Ulke, A. (2006). Phase Distribution in the Cap Bubble Regime in a Duct. *Journal of Fluids Engineering*, *128*(4), 811. https://doi.org/10.1115/1.2201626

Lubchenko, N., Magolan, B., Sugrue, R., & Baglietto, E. (2018). A more fundamental wall lubrication force from turbulent dispersion regularization for multiphase CFD applications. *International Journal of Multiphase Flow*, *98*, 36–44. https://doi.org/10.1016/j.ijmultiphaseflow.2017.09.003

Marfaing, O., Guingo, M., Laviéville, J., Mimouni, S., Baglietto, E., Lubchenko, N., Magolan, B., Sugrue, R., & Nadiga, B. T. (2018). Comparison and uncertainty quantification of two-fluid models for bubbly flows with NEPTUNE_CFD and STAR-CCM+. *Nuclear Engineering and Design*, *337*(December 2017), 1–16. https://doi.org/10.1016/j.nucengdes.2018.05.028

Prabhudharwadkar, D., Vaidheeswaran, A., de Bertodano, M. L., Buchanan, J., & Guilbert, P. (2012). Two-Fluid CFD Simulations of Cap Bubble Flow Using the Two-Group Interfacial Area Transport Equations. *The Journal of Computational Multiphase Flows*, *4*(4), 363–374. https://doi.org/10.1260/1757-482x.4.4.363

Rzehak, R., & Krepper, E. (2013). CFD modeling of bubble-induced turbulence. *International Journal of Multiphase Flow*, *55*, 138–155. https://doi.org/10.1016/j.ijmultiphaseflow.2013.04.007

Sato, Y., & Sekoguchi, K. (1975). Liquid velocity distribution in two-phase bubble flow. *International Journal of Multiphase Flow*, *2*(1), 79–95. https://doi.org/10.1016/0301-9322(75)90030-0

Schiller, L., & Naumann, Z. (1935). A drag coefficient correlation. *Z.Ver.Deutsch.Ing*, *77*(13–14), 318–320. https://doi.org/10.1016/j.ijheatmasstransfer.2009.02.006

Serizawa, A., & Kataoka, I. (1988). Phase distribution in two-phase flow, Transient Phenomena in Multiphase Flow. *Transient Phenomena in Multiphase Flow*, 179–224

Sharma, S. L., Hibiki, T., Ishii, M., Brooks, C. S., Schlegel, J. P., Liu, Y., & Buchanan, J. R. (2017). Turbulence-induced bubble collision force modeling and validation in adiabatic two-phase flow using CFD. *Nuclear Engineering and Design*, *312*, 399–409. https://doi.org/10.1016/j.nucengdes.2016.05.006

Sharma, S. L., Ishii, M., Hibiki, T., Schlegel, J. P., Liu, Y., & Buchanan, J. R. (2019). Beyond bubbly two-phase flow investigation using a CFD three-field two-fluid model. *International Journal of Multiphase Flow*, *113*, 1–15. https://doi.org/10.1016/j.ijmultiphaseflow.2018.12.010

Shaver, D. R., & Podowski, M. Z. (2015). Modeling of Interfacial Forces for Bubbly Flows in Subcooled Boiling Conditions. *Transactions of the American Nuclear Society*, *113*(10), 1368–1371

Stern, F., Wilson, R. V., Coleman, H. W., & Paterson, E. G. (2001). Comprehensive Approach to Verification and Validation of CFD Simulations—Part 1: Methodology and Procedures. *Journal of Fluids Engineering*, *123*(4), 793. https://doi.org/10.1115/1.1412235

Sugrue, R., Magolan, B., Lubchenko, N., & Baglietto, E. (2017). Assessment of a simplified set of momentum closure relations for low volume fraction regimes in STAR-CCM+ and OpenFOAM. *Annals of Nuclear Energy*, *110*, 79–87. https://doi.org/10.1016/j.anucene.2017.05.059

Tomiyama, A., Tamai, H., Zun, I., & Hosokawa, S. (2002). Transverse migration of single bubble in simple shear flows. *Chemical Engineering Science*, *57*, 1849–1858

van Wachem, B. G. M. M., & Almstedt, A. E. (2003). Methods for multiphase computational fluid dynamics. *Chemical Engineering Journal*, *96*(1–3), 81–98. https://doi.org/10.1016/j.cej.2003.08.025

Wu, Q., Kim, S., & Ishii, M. (1998). One-group interfacial area transport in vertical bubbly flow. *Int. J. Heat Mass Transfer.*, *41*(8–9), 1103–1112. https://doi.org/10.1016/S0017-9310(97)00167-1

Yeoh, G. H., & Tu, J. (2010). Future Trends in Handling Turbulent Multi-Phase Flows. In *Computational Techniques for Multiphase Flows* (pp. 567–601). Elsevier. https://doi.org/10.1016/B978-0-08-046733-7.00010-2